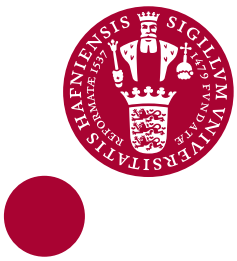

Scalable fabrication of coupled NV center - photonic crystal cavity systems by self-aligned N ion implantation

Schroder, T.; Walsh, M.; Zheng, J.; Mouradian, S.; Li, L.; Malladi, G.; Bakhru, H.; Lu, M.; Stein, A.; Heuck, M.; Englund, D.

Published in:
Optical Materials Express

DOI:
10.1364/OME.7.001514

Publication date:
2017

Document version
Publisher's PDF, also known as Version of record

Research Article | Vol. 7, No. 5 | 1 May 2017 | OPTICAL MATERIALS EXPRESS 1514

Optical Materials EXPRESS

Scalable fabrication of coupled NV center - photonic crystal cavity systems by self-aligned N ion implantation

T. Schröder,[1,2,*] M. Walsh,[1] J. Zheng,[1,3] S. Mouradian,[1] L. Li,[1] G. Malladi,[4] H. Bakhru,[4] M. Lu,[5] A. Stein,[5] M. Heuck,[1] and D. Englund[1]

[1]*Massachusetts Institute of Technology, Research Laboratory of Electronics, 77 Massachusetts Avenue, Cambridge, MA 02139, USA*
[2]*Now at Niels Bohr Institute, University of Copenhagen, Blegdamsvej 17, 2100 Copenhagen, Denmark*
[3]*Department of Electrical Engineering, Columbia University, New York, NY 10027, USA*
[4]*College of Nanoscale Science and Engineering, SUNY Polytechnic Institute, Albany, NY 12203, USA*
[5]*Center for Functional Nanomaterials, Brookhaven National Laboratory, Upton, NY 11973, USA*
[*]*schroder@nbi.ku.dk*

Abstract: Towards building large-scale integrated photonic systems for quantum information processing, spatial and spectral alignment of single quantum systems to photonic nanocavities is required. Here, we demonstrate spatially targeted implantation of nitrogen vacancy (NV) centers into the mode maximum of 2-d diamond photonic crystal cavities with quality factors up to 8000, achieving an average of 1.1 ± 0.2 NVs per cavity. Nearly all NV-cavity systems have significant emission intensity enhancement, reaching a cavity-fed spectrally selective intensity enhancement, F_{int}, of up to 93. Although *spatial* NV-cavity overlap is nearly guaranteed within about 40 nm, spectral tuning of the NV's zero-phonon-line (ZPL) is still necessary after fabrication. To demonstrate *spectral* control, we temperature tune a cavity into an NV ZPL, yielding $F_{\text{int}}^{ZPL} \sim 5$ at cryogenic temperatures.

OCIS codes: (130.0130) Integrated optics; (270.0270) Quantum optics; (160.2220) Defect-center materials; (250.5300) Photonic integrated circuits; (230.5298) Photonic crystals; (350.4238) Nanophotonics and photonic crystals; (220.1920) Diamond machining.

References and links

1. H.-J. Briegel, W. Dür, J. I. Cirac, and P. Zoller, "Quantum Repeaters: The Role of Imperfect Local Operations in Quantum Communication," Phys. Rev. Lett. **81**, 5932–5935 (1998).
2. L. Childress, J. M. Taylor, A. S. Sørensen, and M. D. Lukin, "Fault-tolerant quantum repeaters with minimal physical resources and implementations based on single-photon emitters," Phys. Rev. A **72**, 052330 (2005).
3. K. Nemoto, M. Trupke, S. J. Devitt, B. Scharfenberger, K. Buczak, J. Schmiedmayer, and W. J. Munro, "Photonic Quantum Networks formed from NV- centers," Scientific Reports **6**, 26284 (2016).
4. T. D. Ladd, F. Jelezko, R. Laflamme, Y. Nakamura, C. Monroe, and J. L. O'Brien, "Quantum computers," Nature **464**, 45–53 (2010).
5. C. Monroe, R. Raussendorf, A. Ruthven, K. R. Brown, P. Maunz, L.-M. Duan, and J. Kim, "Large-scale modular quantum-computer architecture with atomic memory and photonic interconnects," Phys. Rev. A **89**, 022317 (2014).
6. K. Nemoto, M. Trupke, S. J. Devitt, A. M. Stephens, B. Scharfenberger, K. Buczak, T. Nöbauer, M. S. Everitt, J. Schmiedmayer, and W. J. Munro, "Photonic Architecture for Scalable Quantum Information Processing in Diamond," Phys. Rev. X **4**, 031022 (2014).
7. H. Bernien, B. Hensen, W. Pfaff, G. Koolstra, M. S. Blok, L. Robledo, T. H. Taminiau, M. Markham, D. J. Twitchen, L. Childress, and R. Hanson, "Heralded entanglement between solid-state qubits separated by three metres," Nature **497**, 86–90 (2013).
8. B. Hensen, H. Bernien, A. E. Dréau, A. Reiserer, N. Kalb, M. S. Blok, J. Ruitenberg, R. F. L. Vermeulen, R. N. Schouten, C. Abellán, W. Amaya, V. Pruneri, M. W. Mitchell, M. Markham, D. J. Twitchen, D. Elkouss, S. Wehner, T. H. Taminiau, and R. Hanson, "Loophole-free Bell inequality violation using electron spins separated by 1.3 kilometres," Nature **526**, 682–686 (2015).
9. A. Faraon, P. E. Barclay, C. Santori, K.-M. C. Fu, and R. G. Beausoleil, "Resonant enhancement of the zero-phonon emission from a colour centre in a diamond cavity," Nat. Photon. **5**, 301–305 (2011).

#284086 https://doi.org/10.1364/OME.7.001514
Journal © 2017 Received 6 Jan 2017; revised 2 Mar 2017; accepted 5 Mar 2017; published 6 Apr 2017

Optical Materials EXPRESS

10. J. Riedrich-Möller, L. Kipfstuhl, C. Hepp, E. Neu, C. Pauly, F. Mücklich, A. Baur, M. Wandt, S. Wolff, M. Fischer, S. Gsell, M. Schreck, and C. Becher, "One- and two-dimensional photonic crystal microcavities in single crystal diamond," Nature Nanotechnology **7**, 69–74 (2012).
11. A. Faraon, C. Santori, Z. Huang, V. M. Acosta, and R. G. Beausoleil, "Coupling of Nitrogen-Vacancy Centers to Photonic Crystal Cavities in Monocrystalline Diamond," Phys. Rev. Lett. **109**, 033604 (2012).
12. B. J. M. Hausmann, B. J. Shields, Q. Quan, Y. Chu, N. P. de Leon, R. Evans, M. J. Burek, A. S. Zibrov, M. Markham, D. J. Twitchen, H. Park, M. D. Lukin, and M. Lončar, "Coupling of NV Centers to Photonic Crystal Nanobeams in Diamond," Nano Lett. **13**, 5791–5796 (2013).
13. L. Li, T. Schröder, E. H. Chen, M. Walsh, I. Bayn, J. Goldstein, O. Gaathon, M. E. Trusheim, M. Lu, J. Mower, M. Cotlet, M. L. Markham, D. J. Twitchen, and D. Englund, "Coherent spin control of a nanocavity-enhanced qubit in diamond," Nat. Commun. **6**, 6173 (2015).
14. M. Gregor, R. Henze, T. Schröder, and O. Benson, "On-demand positioning of a preselected quantum emitter on a fiber-coupled toroidal microresonator," Appl. Phys. Lett. **95**, 153110 (2009).
15. D. Englund, B. Shields, K. Rivoire, F. Hatami, J. Vuckovic, H. Park, and M. D. Lukin, "Deterministic Coupling of a Single Nitrogen Vacancy Center to a Photonic Crystal Cavity," Nano Lett. **10**, 3922–3926 (2010).
16. J. Wolters, A. W. Schell, G. Kewes, N. Nüsse, M. Schoengen, H. Doscher, T. Hannappel, B. Lochel, M. Barth, and O. Benson, "Enhancement of the zero phonon line emission from a single nitrogen vacancy center in a nanodiamond via coupling to a photonic crystal cavity," Appl. Phys. Lett. **97**, 141108 (2010).
17. J. Riedrich-Möller, S. Pezzagna, J. Meijer, C. Pauly, F. Mücklich, M. Markham, A. M. Edmonds, and C. Becher, "Nanoimplantation and Purcell enhancement of single nitrogen-vacancy centers in photonic crystal cavities in diamond," Appl. Phys. Lett. **106**, 221103 (2015).
18. T. Schröder, E. Chen, L. Li, M. Walsh, M. E. Trusheim, I. Bayn, and D. Englund, "Targeted creation and Purcell enhancement of NV centers within photonic crystal cavities in single-crystal diamond," in "Conference on Lasers and Electro-Optics 2014," (OSA, 2014), OSA Technical Digest (online), p. FW1B.6.
19. T. Schröder, L. Li, E. Chen, M. Walsh, M. E. Trusheim, I. Bayn, J. Zheng, S. Mouradian, H. Bakhru, O. Gaathon, and D. R. Englund, "Deterministic High-yield Creation of Nitrogen Vacancy Centers in Diamond Photonic Crystal Cavities and Photonic Elements," in "Conference on Lasers and Electro-Optics 2015," (OSA, 2015), OSA Technical Digest (online), p. FTh3B.1.
20. M. Schukraft, J. Zheng, T. Schröder, S. L. Mouradian, M. Walsh, M. E. Trusheim, H. Bakhru, and D. R. Englund, "Invited Article: Precision nanoimplantation of nitrogen vacancy centers into diamond photonic crystal cavities and waveguides," APL Photonics **1**, 020801 (2016).
21. D. M. Toyli, C. D. Weis, G. D. Fuchs, T. Schenkel, and D. D. Awschalom, "Chip-Scale Nanofabrication of Single Spins and Spin Arrays in Diamond," Nano Lett. **10**, 3168–3172 (2010).
22. I. Bayn, E. Chen, L. Li, M. Trusheim, T. Schröder, O. Gaathon, M. Lu, A. Stein, M. Liu, K. Kisslinger, and D. Englund, "Implantation of proximal NV clusters in diamond by lithographically defined silicon masks with 5 nm resolution," in "CLEO: 2014," (Optical Society of America, 2014), OSA Technical Digest (online), p. FW3B.2.
23. M. Lesik, P. Spinicelli, S. Pezzagna, P. Happel, V. Jacques, O. Salord, B. Rasser, A. Delobbe, P. Sudraud, A. Tallaire, J. Meijer, and J.-F. Roch, "Maskless and targeted creation of arrays of colour centres in diamond using focused ion beam technology," Physica Status Solidi (a) **210**, 2055–2059 (2013).
24. S. Tamura, G. Koike, A. Komatsubara, T. Teraji, S. Onoda, L. P. McGuinness, L. Rogers, B. Naydenov, E. Wu, L. Yan, F. Jelezko, T. Ohshima, J. Isoya, T. Shinada, and T. Tanii, "Array of bright silicon-vacancy centers in diamond fabricated by low-energy focused ion beam implantation," Appl. Phys. Express **7**, 115201 (2014).
25. I. Bayn, E. H. Chen, M. E. Trusheim, L. Li, T. Schröder, O. Gaathon, M. Lu, A. Stein, M. Liu, K. Kisslinger, H. Clevenson, and D. Englund, "Generation of Ensembles of Individually Resolvable Nitrogen Vacancies Using Nanometer-Scale Apertures in Ultrahigh-Aspect Ratio Planar Implantation Masks," Nano Lett. **15**, 1751–1758 (2015).
26. T. Greibe, T. A. Anhøj, L. S. Johansen, and A. Han, "Quality control of JEOL JBX-9500fsz e-beam lithography system in a multi-user laboratory," Microelectron. Eng. **155**, 25–28 (2016).
27. S. Tomljenovic-Hanic, M. J. Steel, C. M. de Sterke, and J. Salzman, "Diamond based photonic crystal microcavities," Opt. Express **14**, 3556 (2006).
28. J. Riedrich-Möller, E. Neu, and C. Becher, "Design of microcavities in diamond-based photonic crystals by Fourier- and real-space analysis of cavity fields," Photonics and Nanostructures - Fundamentals and Applications **8**, 150–162 (2010).
29. Y. Akahane, T. Asano, B.-S. Song, and S. Noda, "High-Q photonic nanocavity in a two-dimensional photonic crystal," Nature **425**, 944–947 (2003).
30. S. Noda, A. Chutinan, and M. Imada, "Trapping and emission of photons by a single defect in a photonic bandgap structure," Nature **407**, 608–610 (2000).
31. T. Schröder, S. L. Mouradian, J. Zheng, M. E. Trusheim, M. Walsh, E. H. Chen, L. Li, I. Bayn, and D. Englund, "Quantum nanophotonics in diamond [Invited]," JOSA B **33**, B65 (2016).
32. L. Li, I. Bayn, M. Lu, C.-Y. Nam, T. Schröder, A. Stein, N. C. Harris, and D. Englund, "Nanofabrication on unconventional substrates using transferred hard masks," Sci. Rep. **5**, 7802 (2015).
33. S. L. Lai, D. Johnson, and R. Westerman, "Aspect ratio dependent etching lag reduction in deep silicon etch processes," Journal of Vacuum Science & Technology A **24**, 1283–1288 (2006).

Optical Materials EXPRESS

34. H. Jansen, M. de Boer, R. Wiegerink, N. Tas, E. Smulders, C. Neagu, and M. Elwenspoek, "RIE lag in high aspect ratio trench etching of silicon," Microelectron. Eng. **35**, 45–50 (1997).
35. J. F. Ziegler, M. D. Ziegler, and J. P. Biersack, "SRIM - The stopping and range of ions in matter (2010)," Nuclear Instruments and Methods in Physics Research B **268**, 1818–1823 (2010).
36. R. Albrecht, A. Bommer, C. Deutsch, J. Reichel, and C. Becher, "Coupling of a Single Nitrogen-Vacancy Center in Diamond to a Fiber-Based Microcavity," Phys. Rev. Lett. **110**, 243602 (2013).
37. E. M. Purcell, "Spontaneous emission probabilities at radio frequencies," Physical Review **69**, 681 (1946).
38. H.-Q. Zhao, M. Fujiwara, and S. Takeuchi, "Suppression of fluorescence phonon sideband from nitrogen vacancy centers in diamond nanocrystals by substrate effect," Opt. Express **20**, 15628 (2012).
39. A. Alkauskas, B. B. Buckley, D. D. Awschalom, and C. G. V. d. Walle, "First-principles theory of the luminescence lineshape for the triplet transition in diamond NV centres," New J. Phys. **16**, 073026 (2014).
40. C. Santori, D. Fattal, and Y. Yamamoto, *Single-photon Devices and Applications* (John Wiley & Sons, 2010).
41. T. G. Tiecke, J. D. Thompson, N. P. de Leon, L. R. Liu, V. Vuletić, and M. D. Lukin, "Nanophotonic quantum phase switch with a single atom," Nature **508**, 241–244 (2014).
42. H. Kaupp, C. Deutsch, H.-C. Chang, J. Reichel, T. W. Hänsch, and D. Hunger, "Scaling laws of the cavity enhancement for NV centers in diamond," arXiv:1304.0948 (2013).
43. R. Albrecht, A. Bommer, C. Pauly, F. Mücklich, A. W. Schell, P. Engel, T. Schröder, O. Benson, J. Reichel, and C. Becher, "Narrow-band single photon emission at room temperature based on a single nitrogen-vacancy center coupled to an all-fiber-cavity," Appl. Phys. Lett. **105**, 073113 (2014).
44. S. Mosor, J. Hendrickson, B. C. Richards, J. Sweet, G. Khitrova, H. M. Gibbs, T. Yoshie, A. Scherer, O. B. Shchekin, and D. G. Deppe, "Scanning a photonic crystal slab nanocavity by condensation of xenon," Appl. Phys. Lett. **87**, 141105 (2005).
45. D. Scarabelli, M. Trusheim, O. Gaathon, D. Englund, and S. J. Wind, "Nanoscale Engineering of Closely-Spaced Electronic Spins in Diamond," Nano Lett. **16**, 4982–4990 (2016).
46. X. Chew, G. Zhou, H. Yu, F. S. Chau, J. Deng, Y. C. Loke, and X. Tang "An in-plane nano-mechanics approach to achieve reversible resonance control of photonic crystal nanocavities," Opt. Express **18**, 22232–22244 (2010).
47. S. L. Mouradian and D. Englund, "A Tunable Waveguide-Coupled Cavity Design for Efficient Spin-Photon Interfaces in Photonic Integrated Circuits," arXiv:1610.08950 [physics, physics:quant-ph] (2016).
48. S. L. Mouradian, T. Schröder, C. B. Poitras, L. Li, J. Goldstein, E. H. Chen, M. Walsh, J. Cardenas, M. L. Markham, D. J. Twitchen, M. Lipson, and D. Englund, "Scalable Integration of Long-Lived Quantum Memories into a Photonic Circuit," Phys. Rev. X **5**, 031009 (2015).

1. Introduction

Efficient interfaces between photons and long-lived spin-based quantum memories are a central requirement for a range of proposed quantum technologies, including quantum repeaters for

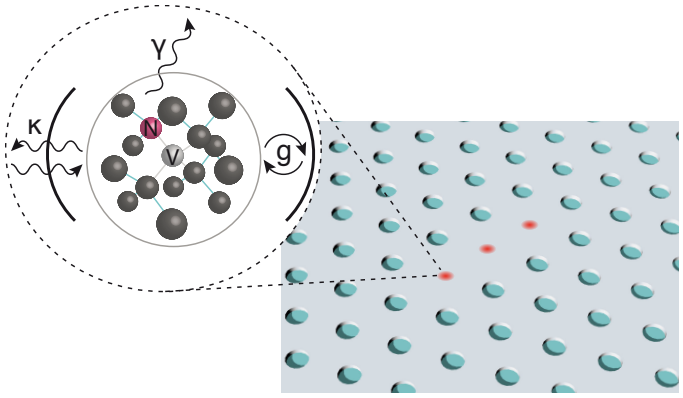

Fig. 1. Illustration of a spin-photon interface. To enable efficient spin—photon interaction, the optical dipole of the associated electron spin is coupled to an optical cavity, here an L3 cavity. The inset schematics shows the nitrogen vacancy (NV) center in diamond coupled to an optical cavity. g, κ, and γ are the Rabi frequency, the cavity dissipation rate, and NV spontaneous emission rate, respectively. N is nitrogen, V vacancy, and the dark gray circles represent carbon.

Optical Materials EXPRESS

long-range quantum communications [1–3] and modular quantum computers [4–6]. There has been much interest in developing such optically connected quantum memories in solid state systems, chiefly among them the nitrogen vacancy (NV) center in diamond, which is distinguished by exceptionally long-lived spin ground states. Recently, the first demonstrations of quantum entanglement between distant diamond NV centers were reported [7], but the rate of heralded entanglement was still smaller than the spin decoherence rate [8], in large part because of inefficient collection of coherent zero-phonon-line (ZPL) radiation from the NV center. Coupling the NV's ZPL to nanocavity resonances (Fig. 1) can greatly improve the efficiency of spin-photon coupling, and a range of all-diamond [9–13] and hybrid NV-cavity systems have been demonstrated [14–16]. However, a remaining challenge for diamond-based cavities is to control the spatial overlap between NV centers and cavity modes. Recently, this problem has been addressed by nitrogen implantation through pierced AFM apertures [17] and implantation through nano-scale apertures of the fabrication mask, where only one mask is used for both implantation into and nanopatterning of the diamond thin film [18–20]. Here, we expand on our recent work [18] on targeted NV generation within 2-dimensional (2-d) photonic crystal cavities (Fig. 2).

Two strategies are being pursued for *spatially* aligning defect centers with photonic nanocavities: (i) the fabrication of a cavity around a pre-selected defect and (ii) the targeted creation of a defect at the mode maximum of a cavity. The targeted creation of diamond defects relative to *each other* has been demonstrated using apertures in masks [21, 22] and focused ion beam implantation with subsequent annealing [23, 24]. The highest positioning precision was achieved using a silicon implantation mask down to 25.8 nm [25] but its application to nanostructures is more challenging: the implantation apertures must exactly target the fabricated nanostructure. This could be realized in a two-step-lithographic process, where precise overlay control is needed between the photonic patterns and implantation apertures. Although recently e-beam overlay accuracy of down to 6 nm was demonstrated [26], such a two-step overlay process is still challenging to implement, requires advanced localization methods, and alignment precision is generally limited to several tens of nanometers in alignment precision.

Here, we introduce in detail a self-aligned lithography technique that was recently proposed by us for diamond thin-films [18, 19] and demonstrated on photonic cavities in bulk diamond [20]. This technique allows for both (i) patterning of nanostructures and (ii) precise implantation with *one* mask as illustrated in Fig. 3. This single mask contains both the nanostructure features on the order of a hundred nanometers, and the circular implantation apertures on the order of a few tens of nanometers. This enables scalable alignment between the implantation apertures and the etch mask with nanometer precision. Thus, spatially deterministic creation of defect centers by ion implantation and subsequent annealing can be achieved. Moreover, this process can be

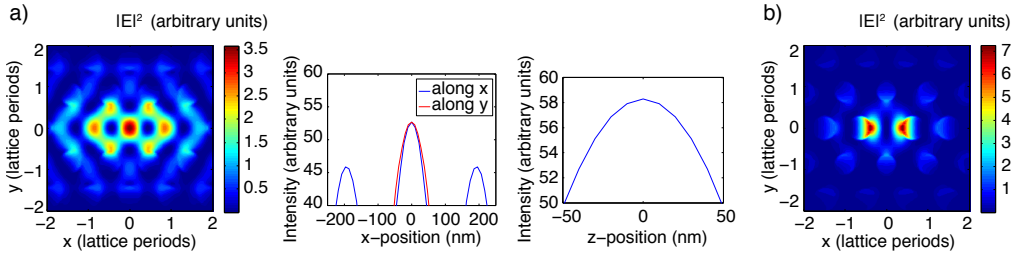

Fig. 2. Design and properties of phonic crystal cavities. a) $|E|^2$ distribution of L3 cavity with three missing holes; design similar to [27]. The left and right inset show a vertical and horizontal cut, respectively. b) $|E|^2$ distribution of M0 cavity with no missing but shifted holes, design similar to [28].

Optical Materials EXPRESS

applied at large scale, enabling scalable, parallel fabrication of a large number of nanostructures with precisely located defect centers — a crucial requirement for large scale quantum photonic systems in quantum information processing. Furthermore, to demonstrate *spectral* control of the NV emission line, we tune a cavity resonance of a second sample into the NV emission line, and demonstrate Purcell enhancement — another crucial requirement for the integration of the NV spin memory into photonic systems.

2. Design of photonic crystal cavities

To demonstrate deterministic implantation of ^{15}N, we choose cavity designs that have high cavity quality (Q) factors, small footprint, and sufficient space between the lattice sites to place implantation apertures at the cavity mode maxima. In principle, a wide range of 1-dimensional (1-d) and 2-d photonic crystal cavities is suitable. Here, we focus on two 2-d photonic crystal lattice defect cavities: (i) an L3 cavity design with three missing holes [27, 29] and (ii) M0 cavities in which the defect is created by shifting the holes around a central region and adjusting their size [28, 30]. The L3 cavity has the advantage that its fundamental mode has three local mode maxima (Fig. 2(a)), hence three implantation holes were added to the mask. This allows equal NV creation probabilities at lower implantation dose compared to the M0 cavity. For the M0 cavity we only implemented a single implantation aperture in its center due to space restrictions (Fig. 2(b)). Keeping the NV density as low as possible is important to reduce spectral diffusion of the ZPL and decoherence of the NV electron spin [31]. On the other hand, the M0 cavity has a small footprint and can theoretically feature Q factors up to 320,000 in diamond as reported by Riedrich-Möller et al. [28]. We use the same design parameters for the fabrication of our L3 and M0 cavities as reported in [27] and [28]. To estimate the precision requirement for implantation, we determine the volume in which the cavity mode intensity exceeds 90% (Fig. 2). For the lateral dimensions of the L3 cavity, for example, this corresponds to ± ~ 35 nm and for the z-direction to ± ~ 40 nm, well within the expected straggle during nitrogen ion implantation.

3. Fabrication

The fabrication scheme is similar to that in Ref. [32] and is illustrated in Fig. 3. We first fabricate a silicon etch mask from 220 nm (and for some samples as indicated 270 nm) silicon-on-insulator (SOI) according to the theoretical design with additional implantation holes with 20 – 35 nm

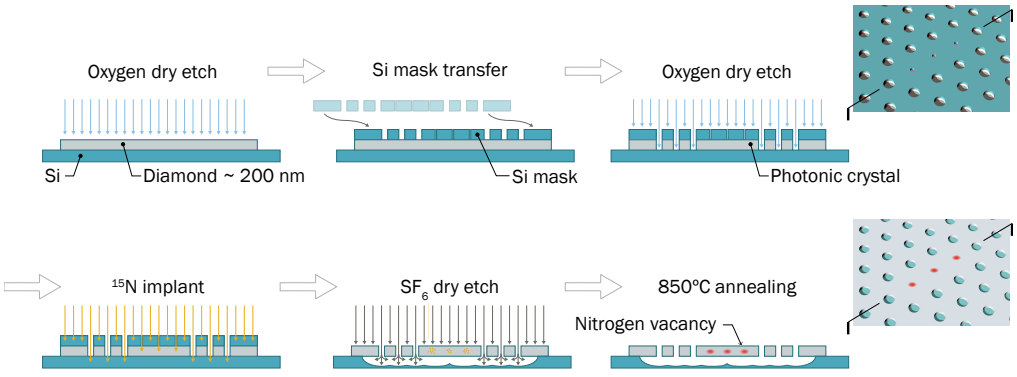

Fig. 3. Illustration of the fabrication process. The sample preparation and nanopatterning are detailed in Ref. [32]. In addition to this method, we use the Si mask both for diamond pattering (step 3, oxygen dry etch) as well as implantation mask for ^{15}N (step 4, implantation). By using the same mask for both steps, we achieve inherent self-alignment of the nanostructure to the implantation aperture.

Optical Materials EXPRESS

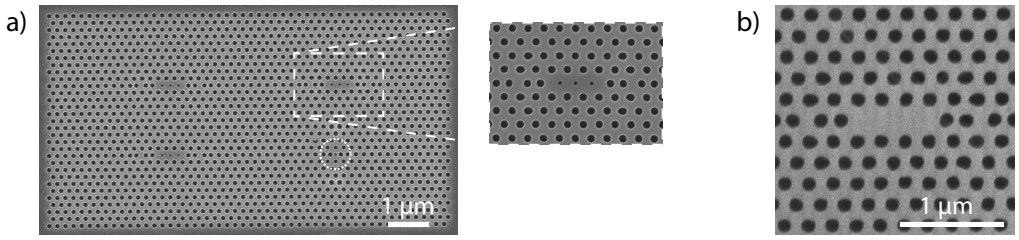

Fig. 4. a) Scanning electron micrograph (SEM) of silicon hard mask for dry etching and ion implantation. The photonic crystal contains three L3 cavities as well as one M0 cavity (bottom right, dotted circle). Inset: Zoom-in. b) SEM of patterned diamond membrane. At the position of the implantation apertures no surface damage is visible, indicating the very slow etch rate due to etching lag reduction [33]. The SEM was not taken on the highest quality sample; samples that showed the reported Q-factors were not imaged in the scanning electron microscope as this can lead to NV charge conversion and even permanent bleaching of the NV.

radii in the center of the cavity defects by standard fabrication processing on SOI. (Fig. 4). This etch mask is placed onto a ~ 200 nm thick diamond membrane. The mask pattern is transferred into the diamond via oxygen reactive ion (RIE) etching; hundreds to thousands of 2-d cavities can be integrated onto a single chip.

The etching rate of holes in an RIE process depends heavily on the aspect ratio of the hole [33, 34]. Thus, we are able to fully transfer our photonic crystal hole features (aspect ratio ~ 2) without etching through the implantation holes (aspect ratio of ~ 4). An SEM of the Si mask is shown in Fig. 4(a)). In independent etch tests with our standard RIE parameters, we find that the diamond surface is not impacted by the RIE patterning process for an upper limit for the aperture radius of ~35 nm for 270 nm thick Si masks corresponding to an aspect ratio of about four. For the 220 nm membrane etch mask we accordingly choose a maximum aperture radius of ~29 nm. After pattern transfer into the diamond, we implant ^{15}N vertically with an ion energy of 40 keV corresponding to an implantation depth of about 40 nm as determined by ion transport calculations (SRIM software package [35]). This does not correspond to the center of the membrane in z-direction and is therefore not the ideal position for maximum coupling; however, due to the limited N ion masking efficiency of the Si mask, we compromise the maximum achievable enhancement for a sample with low number of background NVs. We choose an implantation dosage of $3\text{x}10^{12}/\text{cm}^2$ to target the creation of about one to two NVs per cavity region on average for an NV creation yield of about $1-2\%$. Following the implantation we remove the mask, confirm that the diamond surface at the cavity centers was not impacted by the RIE etching (SEM of diamond membrane in Fig. 4b) and anneal the sample at 850°C to create NVs.

4. NV-cavity system analysis

To determine the yield and position of the NV creation, we perform photoluminescence (PL) measurements in a home-built confocal microscope. Figure 5 illustrates the results: we determine the position of fluorescence spots from single or a few NVs by spectral analysis at the location of the cavity centers as well as throughout the entire photonic crystal area.

These representative PL scans indicate that the probability of finding an NV at an implantation aperture is higher than for the rest of the photonic crystal: we find a significantly higher number of fluorescence spots at the cavity centers. We quantify the number of NVs for the photonic crystal as well as per implantation aperture using second-order auto-correlation measurements. The auto-correlation data allow for relatively precise estimation of the number of NVs if only a

Optical Materials EXPRESS

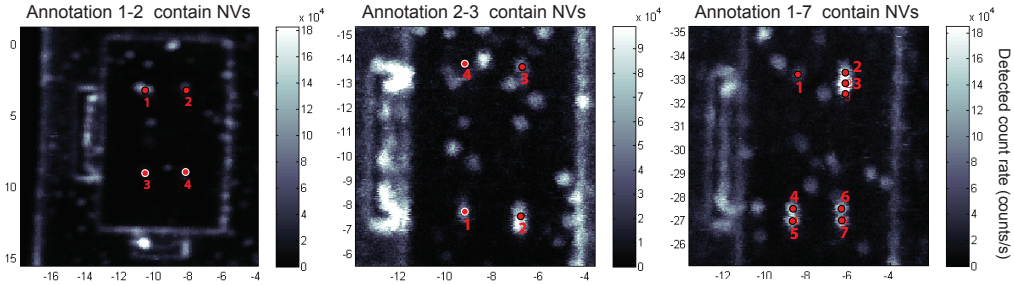

Fig. 5. Photoluminescence raster scans of three different photonic crystal areas with each four cavities (as in Fig. 4(a)) in sample region A. The scan reveals the distribution of fluorescent NV centers. The red dots indicate the approximate position of the cavity maxima where spectra where taken. One or several NVs are indicated by a red dot with black circle, cavity maxima with no NV by red dots with white circle. As expected, at the cavity positions, hence the position of the implantation aperture, the NV density is much higher compared to the photonic crystal region. The unit on the x- and y-axes is μm.

few emitters contribute to the photoluminescence, according to $g^2(\tau = 0) = 1 - (1/N)$ for the ideal case of zero background contribution, where τ is the time difference between detected photon events in an Hanbury Brown and Twiss interferometer, and N is the number of NVs. We also take into consideration a constant background fluorescence that reduces the dip at $\tau = 0$. For the photonic crystal area, we determine a density of randomly distributed NVs of only $0.1 - 0.2$ NV/μm^2. If we extrapolate this density for the cavity area, we expect about $0.04 - 0.08$ NV/cavity, much lower than qualitatively observed in Fig. 5.

We investigate two sample regions with different fabrication parameters. We vary the implantation aperture size to demonstrate control over the average number of NVs per cavity and keep the N ion implantation dose ($3\text{x}10^{12}$/cm^2) and energy (40 keV) equal. For sample region A we anticipated on average 1 NV per cavity, and estimate an average occurrence of 1.1 ± 0.2 per cavity (Fig. 5 and 6, left), deduced from 26 individual implantation spots. This results in $f_{pois}(\lambda = 1.1) \sim 37\%$ cavities coupled to a single NV, assuming a Poisson probability distribution.

Having only one NV per cavity has the advantage of reduced fluorescence background. This is of particular importance as cavity feeding from these additional NVs can substantially contribute

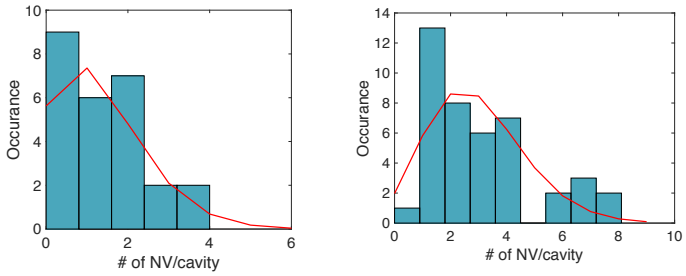

Fig. 6. Statistical analysis of coupled NV-cavity systems. The number of NVs per cavity is plotted and the distribution is fitted according to a Poisson distribution. For sample region A (left plot) and B (right plot) we estimate an average occurrence of 1.1 ± 0.2 and ~3 NVs per cavity, yielding in a ~63% and ~95% probability of finding at least one NV per cavity, respectively. The method for this analysis is detailed in the main text.

Optical Materials EXPRESS

to resonant fluorescence background [36]. The main disadvantage is the relatively low probability of only about 63% for a cavity to contain at least one NV. To increase this probability, we slightly increase the aperture diameter for sample region B (PL scans not shown). We determine an average NV occurrence of ~ 3 per cavity (Fig.6, right), yielding a ~95% probability of finding at least one NV per cavity.

In both sample regions, the NV centers are expected to be distributed within a radius of ~ 42 ± 13 nm for 220 nm thick Si masks. This spatial distribution is determined by the aperture diameter measured with a scanning electron microscope, and an additional lateral straggle (one standard deviation) of ~11 nm for an implantation energy of 40 keV, calculated using SRIM software package [35]. Within a 42 nm radius, the cavity E-field and thereby the Purcell induced rate enhancement only decreases to ~81% of the maximum E-field at the mode maximum as determined with FDTD simulations (Fig. 2). Even taking into account the non-ideal z-localization, the expected E-field is ~ 91 ± 16% of the cavity maximum for 220 nm Si masks.

5. NV-cavity coupling

To show the coupling of the NV to the cavity, we analyze the spectral properties of our NV-cavity systems. We consider two NV-cavity coupling schemes, (i) Purcell enhancement of the spectrally narrow ZPL transition, as well as (ii) phonon-assisted emission enhancement within the phonon sideband (PSB).

The cavity induced spontaneous emission (SE) rate enhancement (i) is described by the Purcell factor [37] given by Eqn. 1. In the case of an NV center, only a few percent of the overall PL is emitted via the ZPL transitions [38]. This reduces coupling of a photon to the ZPL transition. Furthermore, one has to differentiate between the overall Purcell enhancement F and the spectrally-resolved SE rate enhancement $F_{\mathrm{ZPL}} = F/DW$, with DW the Debye-Waller factor, i.e. the intensity ratio of the ZPL to the overall fluorescence [39]. When the NV ZPL is coupled to a cavity with quality factor Q and mode volume V_{mode}, the enhancement is given by

$$F_{\mathrm{ZPL}} = \xi F_{\mathrm{ZPL}}^{\mathrm{max}} \frac{1}{1 + 4Q^2(\lambda_{\mathrm{ZPL}}/\lambda_{\mathrm{cav}} - 1)^2} \tag{1}$$

where $F_{\mathrm{ZPL}}^{\mathrm{max}} = \frac{3}{4\pi^2}\left(\frac{\lambda_{\mathrm{cav}}}{n}\right)^3 \frac{Q}{V_{\mathrm{mode}}}$ is the maximum spectrally-resolved SE rate enhancement [40], $\xi = \left(\frac{|\boldsymbol{\mu}\cdot\mathbf{E}|}{|\boldsymbol{\mu}||\mathbf{E}_{\mathrm{max}}|}\right)^2$ quantifies the angular and spatial overlap between the dipole moment ($\boldsymbol{\mu}$) and the

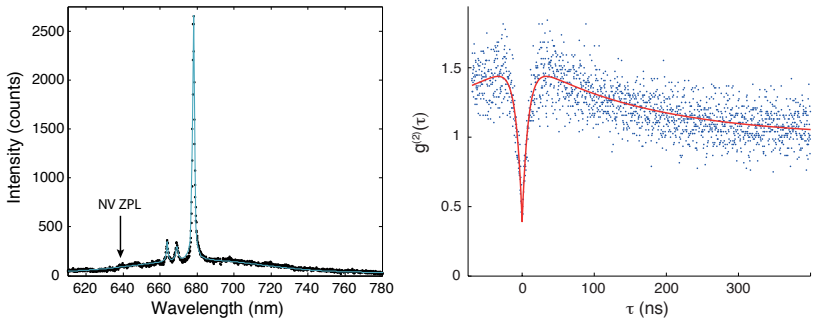

Fig. 7. Spectrum of a single NV coupled to an L3 cavity with an estimated $F_{\mathrm{int}} = 26 \pm 3$. The blue line is a fit to the data with three Lorentian functions for the cavity resonances and a Gaussian function for a simplified representation of the broad NV phonon sideband fluorescence. Comparing the peak maximum intensity with the sideband intensity at the same spectral position yields the given intensity enhancement. Right: Second-order auto-correlation of the cavity coupled single NV. The fit (red curve) yields $g^2(0) \sim 0.38$.

Optical Materials EXPRESS

cavity mode electric field (**E**), and the fraction the spectral overlap between cavity resonance and NV emission wavelength; n is refractive index. In L3 and M0 photonic crystal cavities high $F_{\mathrm{ZPL}}^{\mathrm{max}}$ can be realized due to their small mode volumes [41], $V_{\mathrm{mode}} \sim (\lambda/n)^3$, and their large quality factors as demonstrated here experimentally.

The phonon-assisted emission enhancement (ii) is treated in detail in Ref. [36] and [42]. Albrecht et al. as well as Kaupp et al. show that within the entire NV emission bandwidth the fluorescence emission intensity can be increased around a cavity resonance. Both the ZPL and phonon sidebands contribute to the cavity emission leading to enhancement of the spectral photon rate density [43]. In our analysis of the intensity enhancement, we assume that the collection efficiency from the cavity mode and the uncoupled NV in the photonic crystal are roughly the same. This is justified by the large collection angle of the free space objective with numerical aperture of 0.9.

In Fig. 7 we plot the fluorescence spectrum of a single NV coupled to an L3 cavity. The three cavity modes are spectrally located around 670 nm, close to the maximum of the PSB fluorescence. The mode with $Q = 600 \pm 7$ at 678.1 nm increases the PSB fluorescence by a factor $F_{\mathrm{int}} = 26 \pm 3$ as determined by fitting the cavity modes and NV fluorescence with Lorentzian and a Gaussian function, respectively. Fitting the NV fluorescence with a single Gaussian function only approximates its more complex spectral emission distribution but gives a good estimate for the relevant intensity distribution around the cavity modes. A more detailed model for fitting the NV emission distribution can be found in Ref. [36].

Enhancement of the PSB demonstrates the coupling between the NV and the cavity. However, enhancing the ZPL is much more relevant for improving coherent light-matter interaction. In Fig. 8 we plot the fluorescence spectrum of a single NV coupled to an M0 cavity. Three cavity resonances are spectrally located at 634.9 nm, 638.4 nm, and 655.7 nm, with $Q = 1020$, $Q = 1550$, and $Q = 3950$, respectively. Fitting the data with the same set of functions discussed above, we determine $F_{\mathrm{int}} \sim 12$, $F_{\mathrm{int}} \sim 20$ $F_{\mathrm{int}} \sim 43$. Of particular interest is the cavity resonance at 638.4 nm, which spectrally overlaps with the NV ZPL.

To demonstrate that our method can achieve high localization accuracy, we plot in Fig. 8(b) the spectrum of another cavity-coupled NV PSB that is enhanced through a resonance with $Q = 3280$ at 697.2 nm by a factor $F_{\mathrm{int}} = 93 \pm 7$, indicating that our NV-cavity systems can achieve unprecedented intensity enhancement in nanophotonic devices.

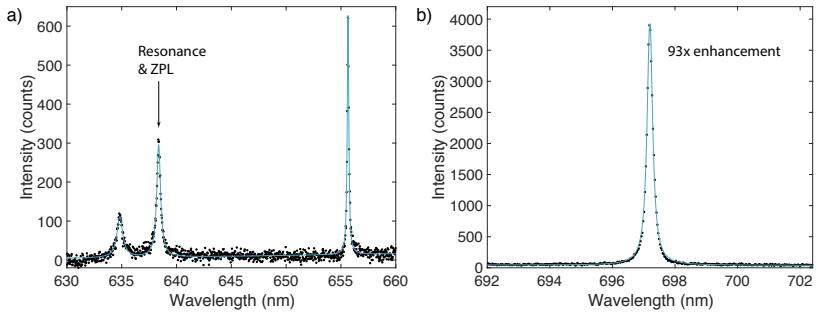

Fig. 8. M0 cavities coupled to single targeted NVs. a) Spectrum of enhanced ZPL at 638 nm and PSB. Several resonances are visible at 634.9 nm, 638.4 nm, and 655.7 nm, with $Q = 1020$, $Q = 1550$, and $Q = 3950$, respectively. Fitting the data as discussed in the main text, we determine $F_{\mathrm{int}} \sim 12$, $F_{\mathrm{int}} \sim 20$ $F_{\mathrm{int}} \sim 43$, respectively, for this single NV. Particularly relevant is the cavity resonance at 638.4 nm where the NV ZPL is located. b) Another single NV—M0 cavity system with narrow resonance ($Q = 3280$) at 697.2 nm enhancing the phonon sideband. Fitting yields an enhancement of the photon rate density by a factor of $F_{\mathrm{int}} = 93 \pm 7$. The blue lines are fits to the data as detailed in the main text.

Optical Materials EXPRESS

6. NV-cavity tuning by temperature control

Besides *spatial* overlap of the NV with the cavity mode maximum, another important requirement for NV-cavity systems is the *spectral* overlap of the NV ZPL emission at 638 nm with a cavity resonance of high Q-factor and the alignment of polarization orientation. Although we are able to fabricate nanocavities with high Q-factors and high spatial overlap, achieving spectral overlap within a few nanometers or even a few ten picometers is still challenging. Tuning the NV ZPL emission line is limited to about ten GHz (~ 14 pm), therefore, tuning of the cavity resonance is required. For diamond systems, the most reliable method has been the controlled gas deposition on the nanostructure to red-tune cavity resonances by desublimation of the gas on the nanostructure [11, 44]. However, the long-term spectral stability of gas tuning suffers from sublimation of ice to gas under laser illumination, leading to a reversal of the tuning.

To demonstrate that diamond cavity resonances can be detuned by temperature control of the sample, we prepared a second sample *without* targeted ^{15}N implantation. The fabrication process is very similar to that described in Sec. 3, with the only difference that the ^{15}N ions are implanted randomly into the diamond before patterning L3 cavities (see Ref. [13]). The spectral properties of one of the fabricated NV-cavity systems at different temperatures are plotted in Fig. 9. The resonance at 638.8 nm has a quality factor of about 8000, determined by fitting a Lorentzian function to the cavity resonance (inset in Fig. 9). This is close to the theoretically expected value [27]. By increasing the temperature by about 6.5 K, we blue-detune this resonance by about 0.16 nm. The achieved overlap leads to a roughly 5-fold intensity enhancement of the ZPL, determined by normalizing the spectra to the intensity of ZPL_1 in Fig. 9 and adjusting the background. ZPL_1 is not coupled to the cavity but spatially located within the optical collection spot. While heating the sample, small drifts relative to the collection spot occurred, leading to slightly different relative intensities of the ZPL_1, ZPL, and cavity peaks, as well as to unstable laser excitation powers. A 5-fold enhancement is small compared to a theoretical maximum of about 470 for an ideal system. We attribute this deviation mainly to spatial and polarization mismatch between NV and cavity - supporting the need for spatially controlled NV generation as discussed above.

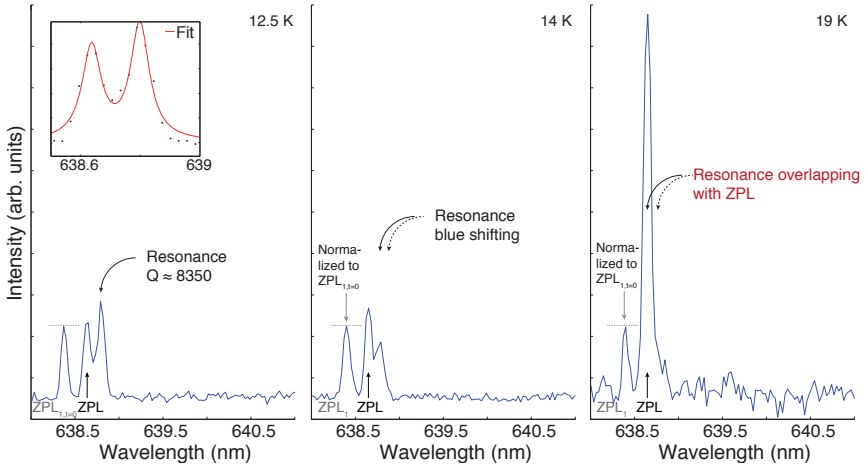

Fig. 9. Temperature tuning of L3 cavity and Purcell enhancement of a single ZPL. This NV, in contrast to the data above was created by random nitrogen implantation before nanofabrication. The spectra at 14 K and 19 K are normalized to the spectrum at 12.5 K via the ZPL_1 intensity. The inset in the left plot indicates a cavity resonance with an estimated quality factor $Q \sim 8000$, indicating the high quality fabrication but at the same time by far non-ideal localization of the NV. The red line is a double Lorentian fit to the data.

Optical Materials EXPRESS

7. Conclusion and outlook

In this letter we introduce a self-aligned lithography technique for the scalable fabrication of hundreds to thousands of NV-cavity systems in diamond. The method can directly be adapted to other defect centers in diamond, such as the silicon or chromium vacancy centers, as well as to other materials in which defect centers can be created by ion implantation; if necessary in combination with subsequent annealing. We demonstrate up to about 90-fold enhancement of the NV emission spectral density. For a single NV-cavity system fabricated without self-aligned lithography, we demonstrate spectral tuning of the resonance and Purcell enhancement of the NV ZPL. The demonstrated emission enhancement, the spectral control at cryogenic temperatures, and the parallel fabrication of large numbers of NV-cavity systems marks an important step towards the fabrication of large arrays of cavity based quantum memories.

Still, there are several remaining challenges. The achieved spatial resolution was limited to about 42 nm. Using thinner masks [45], or by reducing the implantation hole diameter by post-etching atomic-layer deposition [25], better than 30 nm resolution is feasible. To overcome the limited implantation energy of 40 keV caused by the finite masking efficiency of the Si mask, and to implant the N ions with higher energy into the center of the cavity mode maximum, masks with higher extinction [45] could be applied. The thermal tuning method applied for spectral alignment of the cavity resonance to the ZPL is not scalable. To overcome this limitation, spectral tuning capabilities for each individual cavity need to be realized. This requires fabrication of more sophisticated systems, for example systems that allow for micro-electromechanical tuning [46,47].

One of the possible next steps towards realizing the required infrastructure for on-chip quantum networks and quantum processing devices could be the combination of the demonstrated large scale NV-cavity system fabrication with the scalable integration into photonic architectures [48].

Funding

Fabrication and experiments were supported in part by the Air Force Office of Scientific Research (AFOSR) PECASE supervised by Dr Gernot Pomrenke, the AFOSR Quantum Memories MURI, and the U.S. Army Research Laboratory (ARL) Center for Distributed Quantum Information (CDQI). Fabrication was carried out in part at the Center for Functional Nanomaterials, Brookhaven National Laboratory, which is supported by the US DOE, Office of Basic Energy Sciences, under Contract No. DE-SC0012704. MH acknowledges the Danish Council for Independent Research, DFF: 1325-00144.